

## Article

# TiO<sub>2</sub> Nanowires on TiO<sub>2</sub> Nanotubes Arrays (TNWs/TNAs) Decorated with Au Nanoparticles and Au Nanorods for Efficient Photoelectrochemical Water Splitting and Photocatalytic Degradation of Methylene Blue

Ngo Ngoc Uyen <sup>1,2</sup>, Le Thi Cam Tuyen <sup>3</sup>, Le Trung Hieu <sup>4</sup>, Thi Thu Tram Nguyen <sup>5</sup>, Huynh Phuong Thao <sup>6,7</sup>, Tho Chau Minh Vinh Do <sup>6</sup>, Kien Trung Nguyen <sup>8</sup>, Nguyen Thi Nhat Hang <sup>9</sup>, Sheng-Rui Jian <sup>10</sup>, Ly Anh Tu <sup>1,\*</sup>, Phuoc Huu Le <sup>2,\*</sup> and Chih-Wei Luo <sup>11,12,13,14</sup>

**Citation:** Uyen, N.N.; Tuyen, L.T.C.; Hieu, L.T.; Nguyen, T.T.T.; Thao, H.P.; Do, T.C.M.V.; Nguyen, K.T.; Hang, N.T.N.; Jian, S.-R.; Tu, L.A.; et al. TiO<sub>2</sub> Nanowires on TiO<sub>2</sub> Nanotubes Arrays (TNWs/TNAs) Decorated with Au Nanoparticles and Au Nanorods for Efficient Photoelectrochemical Water Splitting and Photocatalytic Degradation of Methylene Blue. *Coatings* **2022**, *12*, 1957. <https://doi.org/10.3390/coatings12121957>

Academic Editor: Alexandru Enesca

Received: 23 October 2022

Accepted: 8 December 2022

Published: 13 December 2022

**Publisher's Note:** MDPI stays neutral with regard to jurisdictional claims in published maps and institutional affiliations.



**Copyright:** © 2022 by the author. Licensee MDPI, Basel, Switzerland. This article is an open access article distributed under the terms and conditions of the Creative Commons Attribution (CC BY) license (<https://creativecommons.org/licenses/by/4.0/>).

- <sup>1</sup> Faculty of Applied Science, Ho Chi Minh City University of Technology-VNUHCM, 268 Ly Thuong Kiet Street, District 10, Ho Chi Minh City 70000, Vietnam
  - <sup>2</sup> Department of Physics and Biophysics, Faculty of Basic Sciences, Can Tho University of Medicine and Pharmacy, 179 Nguyen Van Cu Street, Can Tho City 94000, Vietnam
  - <sup>3</sup> Faculty of Chemical Engineering, Can Tho University, 3/2 Street, Ninh Kieu District, Can Tho City 94000, Vietnam
  - <sup>4</sup> Department of Materials Science and Engineering, National Yang Ming Chiao Tung University, Hsinchu 30010, Taiwan
  - <sup>5</sup> Department of Chemistry, Faculty of Basic Sciences, Can Tho University of Medicine and Pharmacy, 179 Nguyen Van Cu, Can Tho 94000, Vietnam
  - <sup>6</sup> Department of Drug Quality Control-Analytical Chemistry-Toxicology, Faculty of Pharmacy, Can Tho University of Medicine and Pharmacy, 179 Nguyen Van Cu Street, Can Tho City 94000, Vietnam
  - <sup>7</sup> Faculty of Pharmacy, Nam Can Tho University, 168 Nguyen Van Cu (Ext) Street, Can Tho City 94000, Vietnam
  - <sup>8</sup> Department of Physiology, Faculty of Medicine, Can Tho University of Medicine and Pharmacy, 179 Nguyen Van Cu, Can Tho 94000, Vietnam
  - <sup>9</sup> Institute of Applied Technology, Thu Dau Mot University, Thu Dau Mot City 820000, Vietnam
  - <sup>10</sup> Department of Materials Science and Engineering, I-Shou University, Kaohsiung 84001, Taiwan
  - <sup>11</sup> Department of Electrophysics, National Yang Ming Chiao Tung University, Hsinchu 30010, Taiwan
  - <sup>12</sup> National Synchrotron Radiation Research Center, Hsinchu 30076, Taiwan
  - <sup>13</sup> Institute of Physics and Center for Emergent Functional Matter Science, National Yang Ming Chiao Tung University, Hsinchu 30010, Taiwan
  - <sup>14</sup> Department of Physics, University of Washington, Seattle, WA 98195, USA
- \* Correspondence: [lyanhtu@hcmut.edu.vn](mailto:lyanhtu@hcmut.edu.vn) (L.A.T.); [lhuuphuoc@ctump.edu.vn](mailto:lhuuphuoc@ctump.edu.vn) (P.H.L.); Tel.: +84-29-2373-9730 (P.H.L.)

**Abstract:** In this study, TiO<sub>2</sub> nanowires on TiO<sub>2</sub> nanotubes arrays (TNWs/TNAs) and Au-decorated TNWs/TNAs nanostructures are designed and fabricated as a new type of photoanode for photoelectrochemical (PEC) water splitting. The TNWs/TNAs were fabricated on Ti folds by anodization using an aqueous NH<sub>4</sub>F/ethylene glycol solution, while Au nanoparticles (NPs) and Au nanorods (NRs) were synthesized by Turkevich methods. We studied the crystal structure, morphology, and PEC activity of four types of nanomaterial photoanodes, including TNWs/TNAs, Au NPs-TNWs/TNAs, Au NRs-TNWs/TNAs, and Au NPs-NRs-TNWs/TNAs. The TiO<sub>2</sub> and Au-TiO<sub>2</sub> samples exhibited pure anatase phase of TiO<sub>2</sub> with (0 0 4), (1 0 1), and (1 0 5) preferred orientations, while Au-TiO<sub>2</sub> presented a tiny XRD peak of Au (111) due to a small Au decorated content of 0.7 ± 0.2 at.%. In addition, the samples obtained a well-defined and uniform structure of TNAs/TNWs; Au NPs (size of 19.0 ± 1.9 nm) and Au NRs (width of 14.8 ± 1.3 nm and length of 99.8 ± 15.1 nm) were primarily deposited on TNWs top layer; sharp Au/TiO<sub>2</sub> interfaces were observed from HRTEM images. The photocurrent density (*J*) of the photoanode nanomaterials was in the range of 0.24–0.4 mA/cm<sup>2</sup>. Specifically, Au NPs-NRs-decorated TNWs/TNAs attained the highest *J* value of 0.4 mA/cm<sup>2</sup> because the decoration of Au NPs and Au NRs mixture onto TNWs/TNAs improved

the light harvesting capability and the light absorption in the visible-infrared region, enhanced photogenerated carriers' density, and increased electrons' injection efficiency via the localized surface plasmon resonance (LSPR) effect occurring at the Au nanostructures. Furthermore, amongst the investigated nanophotocatalysts, the Au NPs-NRs TNWs/TNAs exhibited the highest photocatalytic activity in the degradation of methylene blue with a high reaction rate constant of  $0.7 \pm 0.07 \text{ h}^{-1}$ , which was 2.5 times higher than that of the pristine TNWs/TNAs.

**Keywords:** Au nanomaterials; anodic TiO<sub>2</sub>; photoelectrochemical water splitting; localized surface plasmon effect; photocatalysts

## 1. Introduction

Since the discovery of photoelectrochemical (PEC) water splitting using a TiO<sub>2</sub> electrode in 1972 [1,2], this effect has widely become a promising route for hydrogen generation. In recent years, global environmental problems are becoming more and more concerned due to severe pollution, especially organic pollutants. During the dyeing process in the textile industry, a large amount (~15%) of total world dye is lost and released in the textile effluents [3]. When the colored wastewaters are discharged into the aquatic environment, it becomes a source of non-aesthetic pollution and causes eutrophication as well as perturbations to the aquatic life.

Semiconductor metal oxides offer a promising method for wastewater treatment and the environmentally friendly production of hydrogen [4,5]. Among different semiconductors, TiO<sub>2</sub> presents exceptional electrochemical and photocatalyst characteristics because of its intriguing electrical and optical properties [5,6]. TiO<sub>2</sub> also possesses excellent chemical- and photo-stability, cost-effectiveness, and nontoxicity, which is suitable for PEC and photocatalytic applications [5–7]. Furthermore, one-dimensional (1D) nanostructures such as TiO<sub>2</sub> nanotubes arrays (TNAs), TiO<sub>2</sub> nanowires on TiO<sub>2</sub> nanotubes arrays (TNWs/TNAs) and TiO<sub>2</sub> nanorods provide a direct conduction pathway for the photogenerated that can improve charge transport and reduce the recombination rate of electron-hole pairs [2,8–11]. However, TiO<sub>2</sub> had a wide band gap of ~3.2 eV for anatase phase, thus it only absorbs the ultraviolet (UV) light, which only accounts for 3–5% of the total sunlight [2,11,12]. An approach for enhancing the visible-light (Vis) photoactivity of TiO<sub>2</sub> is the decoration of noble metal nanostructures with TiO<sub>2</sub> by utilizing the plasmonic effect [2,7,11,13–17]. The use of noble metal nanostructures as a decoration component for TiO<sub>2</sub> offers better photostability as compared with the use of semiconductor quantum dots with the anodic corrosion drawback [9,18,19]. For localized surface plasmon resonance (LSPR), the oscillation frequency is sensitively affected by the size, the shape of metal nanostructures and the dielectric constant of the surrounding environment [20–22]. The Au nanostructures with LSPR act as an antenna to localize the optical energy and sensitize TiO<sub>2</sub> by light with energy below the band gap. Consequently, they generate additional charge carriers for water oxidation or produce additional highly active free radicals such as hydroxyl ( $\cdot\text{OH}$ ) and superoxide ( $\cdot\text{O}_2^-$ ). It has been reported that several unique Au/TiO<sub>2</sub> composite systems achieved significant photoactivity enhancements for efficient solar water splitting owing to the LSPR effect [2,11,17,23] and for photocatalytic degradation pollutants [14,16,24]. For instance, the LSPR-induced electric field amplification near the TiO<sub>2</sub> surface allowed the enhancing of the 66-fold-PEC water splitting performance of Au NP-deposited TiO<sub>2</sub> films under Vis-light illumination [23].

The photoactivity of TiO<sub>2</sub> is enhanced by exploiting the LSPR absorption of Au NPs in the Vis region (typically ~550 nm) [25–28], while the infrared (IR) region of the sunlight spectrum was not utilized fully. Previous studies on Au nanorods (NRs) found that the LSPR absorption in the IR range of Au NRs can be tuned by controlling the aspect ratio and the medium dielectric constant [29–31]. Herein, we demonstrate that the photoactiv-

ity of TiO<sub>2</sub> with Au NPs and Au NRs enhances significantly via monitoring the PEC performance and degradation rate of methylene blue (MB) under UV-Vis irradiation. In this study, we are particularly interested in the TiO<sub>2</sub> nanowires on TiO<sub>2</sub> nanotube arrays (TNWs/TNAs) films fabricated by the anodic oxidation on immobilized titanium folds, since the material can provide a unidirectional electrical channel, large surface-to-volume ratio, and a higher photocatalytic performance than the well-known TNAs [10,14]. This study provides the detailed preparations and characterizations of various Au-TiO<sub>2</sub> nanostructured films, and the mechanism for the enhanced PEC and photocatalytic properties of the Au-TiO<sub>2</sub> systems.

## 2. Materials and Methods

### 2.1. Preparation of TiO<sub>2</sub> Nanowires on TiO<sub>2</sub> Nanotubes Arrays (TNWs/TNAs)

TNWs/TNAs were fabricated on titanium (Ti) foil substrates (10 mm × 25 mm × 0.4 mm, 99.9% purity,) by anodic oxidation. Before anodization, the substrate was first ultrasonically cleaned using acetone, methanol, and deionized (DI) water, and then dried by N<sub>2</sub> gas flow. The anodization was conducted using a two-electrode system with the Ti foil as an anode and a stainless-steel foil (SS304) as a cathode (Figure 1a). The electrolyte included ethylene glycol (97 vol%) with additions of 3 vol% DI water and 0.5 wt.% NH<sub>4</sub>F (SHOWA, Tokyo, Japan). The anodizing voltage and time were 30 V and 5 h to grow TNWs/TNAs. To induce crystallization for TiO<sub>2</sub>, the samples were annealed at 400 °C for 2 h in the air.

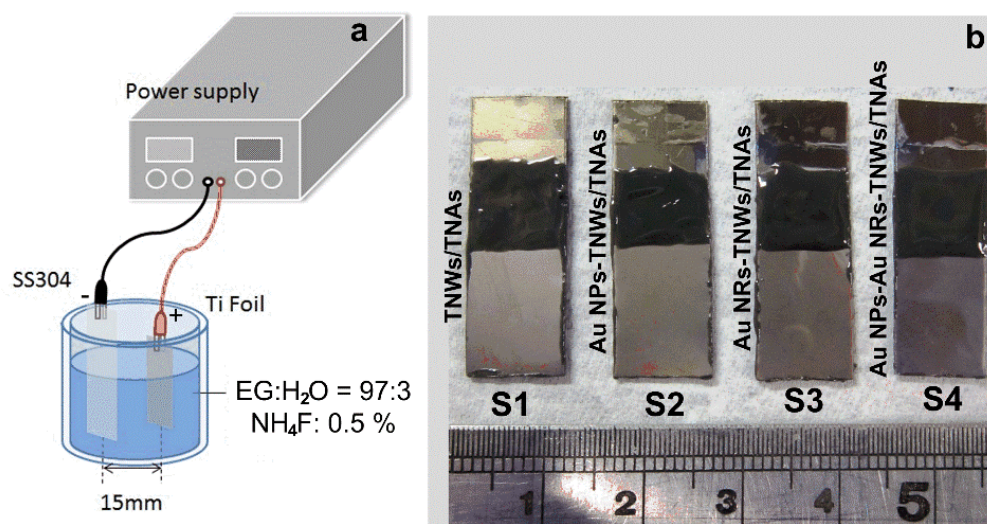


**Figure 1.** (a) A schematic of an electrochemical anodization process. (b) A picture of as-prepared TNWs/TNAs, Au NPs-TNWs/TNAs, Au NRs-TNWs/TNAs, and Au NPs-NRs-TNWs/TNAs.

### 2.2. Synthesis of Au Nanoparticles and Au Nanorods

Au nanoparticles (NPs) were synthesized by the Turkevick method [32,33]. In a typical experiment, 10 mL deionized (DI) water and 100  $\mu$ L of 25 mM HAuCl<sub>4</sub>·3H<sub>2</sub>O (Merck) were placed in a conical flask. The solution was heated to boiling, and 300  $\mu$ L of 1% trisodium citrate was added to the solution under vigorous stirring. The color of the solution immediately changed to light red, which indicates the formation of Au NPs. After continuing the vigorous stirring for 5 min, the solution was cooled to room temperature.

For synthesizing Au nanorods (NRs), a seed solution was first prepared by slowly mixing 100  $\mu$ L of 0.025 M HAuCl<sub>4</sub>·3H<sub>2</sub>O with 10 mL of 0.1 M hexadecyltrimethylammonium bromide (CTAB) in a test tube. Then, 640  $\mu$ L of 0.01 M ice-cold NaBH<sub>4</sub> solution, which was freshly prepared with 100 mL of 0.01 M NaOH and 3.78 mg NaBH<sub>4</sub>, was added all at once under stirring for 30 min. The color of the mixture changed from light yellow

to light brown. A growth solution of Au NRs was prepared by adding 1.75  $\mu\text{M}$   $\text{AgNO}_3$  to a mixture of 1 mM CTAB, 2.5  $\mu\text{M}$   $\text{HAuCl}_4 \cdot 3\text{H}_2\text{O}$  and 50  $\mu\text{M}$  hydroquinone. Finally, 80  $\mu\text{L}$  seed solution was added to the growth solution and left overnight before cleaning through two centrifugation cycles of 10,000 rpm for 20 min.

### 2.3. Preparation of Au NPs-, Au NRs-, and Au-NRs-NPs-Decorated TNWs/TNAs

Au NPs-decorated-TNWs/TNAs ( $S_2$ ), Au NRs-decorated-TNWs/TNAs ( $S_3$ ) and Au NPs-NRs-decorated-TNWs/TNAs ( $S_4$ ) were prepared by drop casting technique using 1 mL Au NPs solution, 1 mL Au NRs solution, and a mixture of 0.5 mL Au NPs and 0.5 mL Au NRs solution, respectively (Figure 1b). The samples were then heated at 120  $^\circ\text{C}$  for 60 min for drying, removing the residual solvent, and improving the connectivity at Au/ $\text{TiO}_2$  interfaces.

### 2.4. Characterization Methods

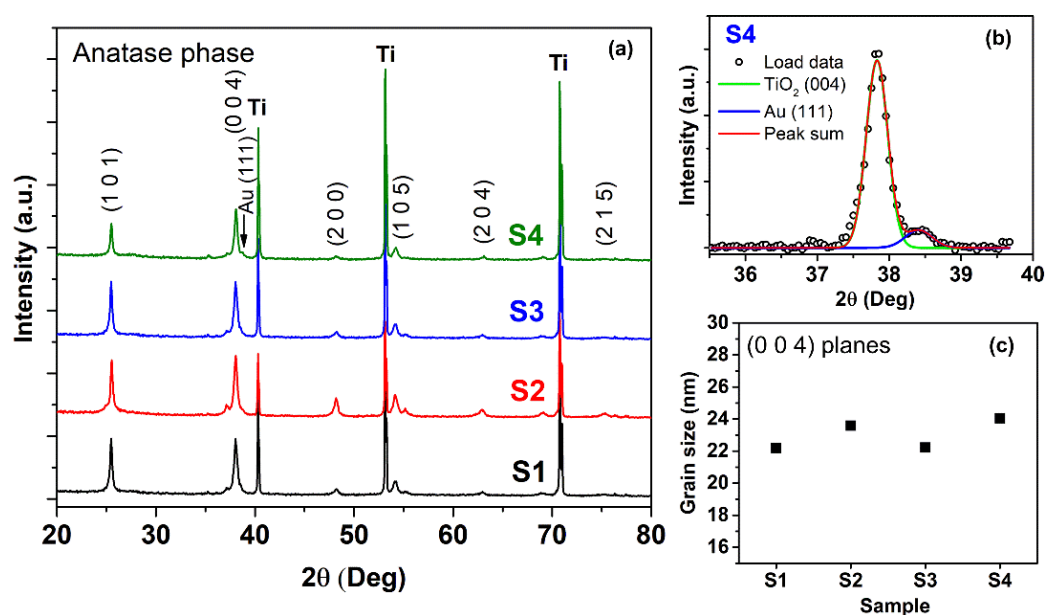
The orientation and crystallinity of the materials will be determined using X-ray diffraction (XRD) (XRD, Bruker D2, Billerica, MA, USA) and using  $\text{Cu K}\alpha$  radiation ( $\lambda = 1.5406 \text{ \AA}$ ) in the  $\theta$ - $2\theta$  configuration. The grain sizes can be estimated by the Scherrer formula. Morphologies and film thicknesses of the samples were characterized by scanning electron microscopy (SEM, JEOL JSM-6500, Pleasanton, CA, USA). The compositions of samples were analyzed using an energy-dispersive X-ray spectroscopy (EDS) equipped with the SEM instrument. The elemental atomic percentage of each sample was obtained by averaging the values measured at 5 distinct  $10 \mu\text{m} \times 12 \mu\text{m}$  areas on the film's surfaces. Structural characterization at atomic scale was performed in a JEOL JEM-ARM200F (Tokyo, Japan) high-resolution scanning transmission electron microscope (HRTEM), operated at 200 kV. A TEM specimen was prepared by scratching the film surface using a pointed diamond tip and transferring the fragments onto a Cu grid. To study the elemental composition and chemical state of the materials, X-ray photoelectron spectra of a selected Au- $\text{TiO}_2$  film were performed by an XPS instrument (ThermoVG 350, East Grinstead, UK) with an X-ray source of  $\text{Mg K}\alpha$  1253.6 eV and 300 W. The  $\text{C}1\text{s}$  peak at 284.8 eV was used as an internal standard, and the freeware XPSPEAK 4.1 was employed for XPS curve fitting with the Shirley background subtraction and assuming a Gaussian-Lorentzian peak shape.

Photoelectrochemical measurements were conducted using a three-electrode cell with a reference electrode of  $\text{Ag}/\text{AgCl}$ , a counter electrode of Pt, and 0.5 M  $\text{Na}_2\text{SO}_4$  electrolyte. The working electrodes were the TNWs/TNAs and Au-TNWs/TNAs films on Ti metal substrate. The substrate edges and the metal contact region were sealed with insulating epoxy resin to leave a working electrode area of  $1.0 \text{ cm}^2$ . Linear sweeps and  $J$ - $t$  scans were measured by an electrochemical workstation (Jiehan 5000, Jiehan Technology Co., Taichung, Taiwan). Incident photon to current conversion efficiencies spectra were collected under illumination light from a 100 W xenon lamp. The photocatalytic activity of the selected films was determined by the decomposition of methylene blue (MB) under UV-VIS irradiation from a 100 W xenon lamp. Prior to illumination, investigated samples were immersed in a MB solution (10 mg/L or  $3.13 \times 10^{-5} \text{ M}$ ) in the dark for 20 min to achieve absorption-desorption equilibrium. All photocatalytic reactions were maintained at 32–34  $^\circ\text{C}$ . After a certain photocatalytic reaction time, 1 mL MB was withdrawn to determine the relative concentration by measuring absorption spectra in the wavelength range of 400–800 nm using a UV-Vis spectrophotometer (Hitachi U-2900, Hitachi, Tokyo, Japan). This spectrophotometer was also used to measure the absorption spectra of the TNWs/TNAs and Au-TNWs/TNAs samples.

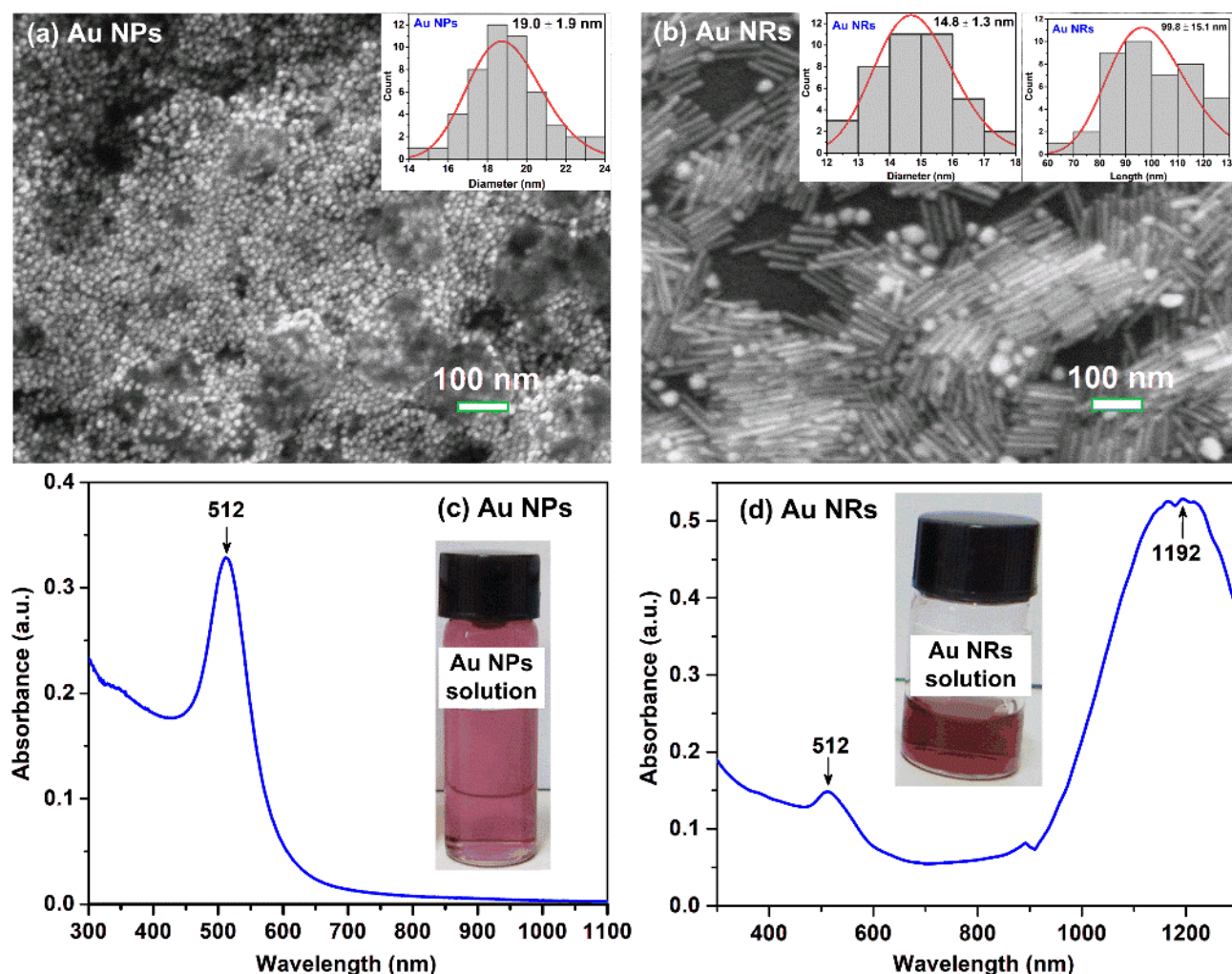
### 3. Results and Discussion

Figure 2 presents the XRD patterns of TNWs/TNAs, Au NPs-TNWs/TNAs, Au NRs-TNWs/TNAs, and Au NPs-NRs-TNWs/TNAs. All the samples exhibited the anatase phase of TiO<sub>2</sub> with preferred lattice planes of (101) at 25.1°, (004) at 37.8°, and (105) at 53.8° (JCPDS No. 21-1272). In addition, there was no rutile TiO<sub>2</sub> phase peak, confirming that the TiO<sub>2</sub> nanomaterials in this study were pure anatase phases. These XRD results are similar to those reported in Refs. [14,34–36] for TiO<sub>2</sub> and Au-TiO<sub>2</sub> nanostructures. A closer inspection of the (004) peaks of Au-TiO<sub>2</sub> samples, Au (111) component was observed by the shoulder peak at 38.3°. Indeed, the fittings of Au-TiO<sub>2</sub> (004) peaks allowed us to extract Au (111) components, as demonstrated in Figure 2b for Au NPs-NRs-TNWs/TNAs (S<sub>4</sub>). This confirms the presence of crystalline Au nanomaterials in S<sub>2</sub>, S<sub>3</sub>, S<sub>4</sub> samples. We employed the Scherrer equation to estimate the grain sizes (*D*) of the samples,  $D = 0.9\lambda/\beta\cos\theta$ , where  $\lambda$ ,  $\beta$ , and  $\theta$  are the X-ray wavelength, full width at half maximum of the TiO<sub>2</sub> (004) peak, and Bragg diffraction angle, respectively [14,37]. As a result, the *D* values varied in a narrow range of 22.2–24.0 nm (Figure 2c), suggesting a similar grain size and crystallinity level amongst the four nanomaterials.

Figure 3 shows the morphologies and absorption spectra of as-prepared Au NPs and Au NRs colloidal solutions. The Au NPs had a uniform spherical shape with a size of  $19.0 \pm 1.9$  nm (Figure 3a), which induced an LSPR peak at 512 nm (Figure 3c), which was consistent with the LSPR-peaks of Au NPs in Refs. [15,38]. Meanwhile, Au NRs exhibited well-defined rods with a length of  $99.8 \pm 15.1$  nm and a width of  $14.8 \pm 1.3$  nm (Figure 3b); they also include a minor amount of Au NPs with an average size of 19.6 nm (Figure 3b). Consequently, the Au NRs had a strong broad LSPR absorption peak at 1192 nm in the infrared region, and a small absorption peak at 512 nm due to the presence of a small amount of Au NPs (Figure 3b,d). The insets in Figure 3c,d are the photographs of the Au NPs and Au NRs colloidal solutions, which exhibit as light red and light brown, respectively. The LSPR peak of Au NPs was consistent with those in refs. [15,38], but the present Au NRs peak at 1192 nm is longer than the Au NRs peaks (range of 740–840 nm) in ref. [30], owing to the differences in the length, width, and aspect ratio of the Au NRs. The interesting optical properties of the Au nanomaterials with LSPR peaks in Vis and/or IR regions are of great interest for their use for enhancing the PEC and photocatalytic activities of the Au-TiO<sub>2</sub> heterostructures (see later).

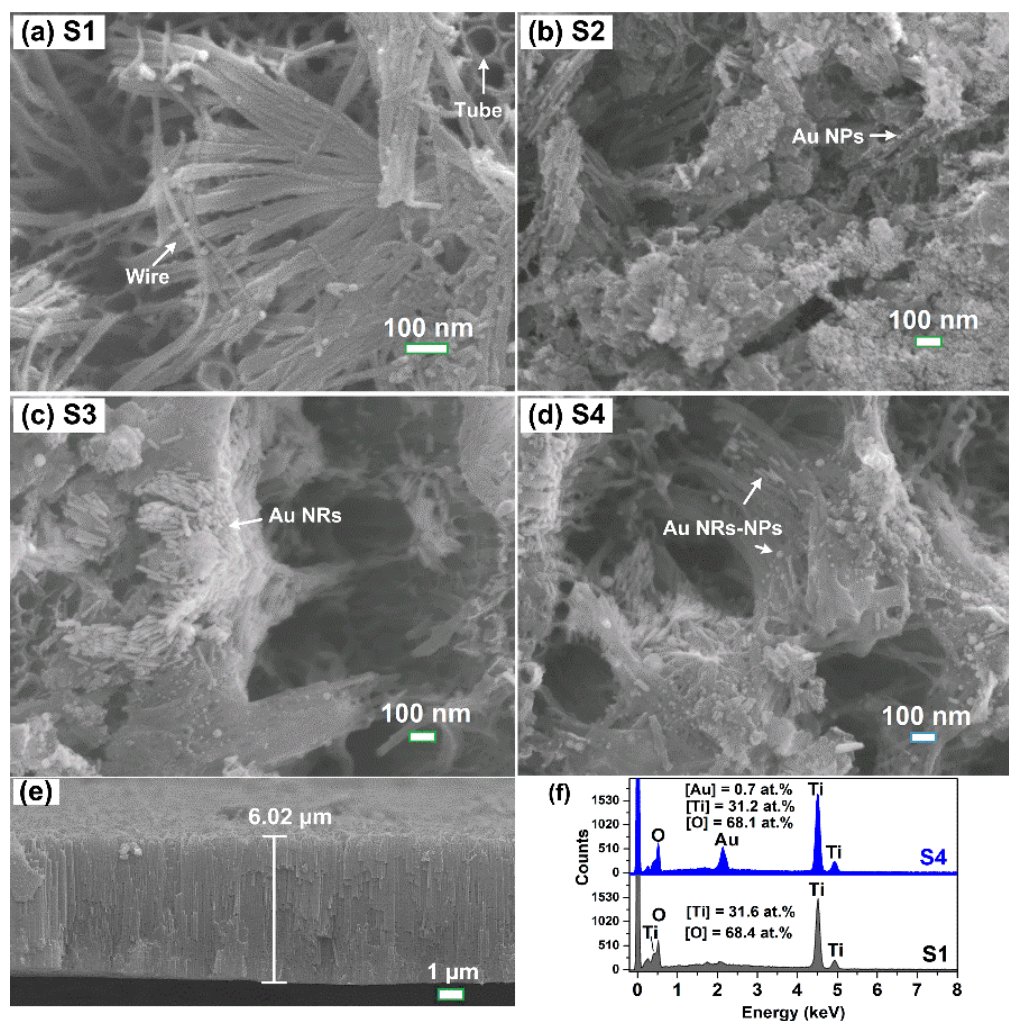


**Figure 2.** (a) The XRD patterns of TNWs/TNAs (S<sub>1</sub>), Au NPs-TNWs/TNAs (S<sub>2</sub>), Au NRs-TNWs/TNAs (S<sub>3</sub>), and Au NPs-NRs-TNWs/TNAs (S<sub>4</sub>). (b) The (004) peak of S<sub>4</sub> shows two components of TiO<sub>2</sub> (004) and Au (111). (c) The estimated grain size of the four nanomaterials.



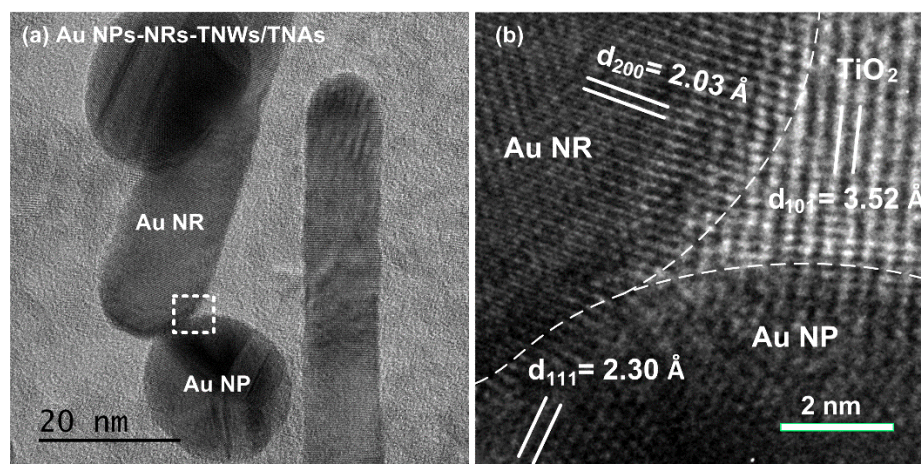
**Figure 3.** (a,b) SEM images of as-prepared Au nanoparticles and Au nanorods colloidal solutions. The insets in (a,b) are the size distribution histograms of Au NPs and Au NRs. (c,d) Absorption spectra of Au nanoparticles and Au nanorods solutions, showing a localized surface plasmon resonance (LSPR) peak at 512 nm for Au NPs, and two peaks at 512 nm and 1192 nm for Au NRs; the insets in (c,d) are the corresponding photographs of the Au NPs and Au NRs solutions.

Figure 4 presents the morphologies of TNWs/TNAs, Au NPs-TNWs/TNAs, Au NRs-TNWs/TNAs, and Au NPs-NRs-TNWs/TNAs. Obviously, the TNWs/TNAs exhibited well-defined nanowires (length of  $\sim 6.0 \mu\text{m}$ ) covering nanotube arrays (tube diameter of  $\sim 80 \text{ nm}$  and length of  $\sim 6.0 \mu\text{m}$ , Figure 4a,e). For Au-TNWs/TNAs samples ( $S_2$ ,  $S_3$ ,  $S_4$ ), Au NPs distributed relatively uniformly on TNWs/TNAs surfaces (Figure 4b). Similarly,  $S_3$  exhibited Au NRs-decoration on TNWs/TNAs surface (Figure 4c), meanwhile  $S_4$  had both Au NPs and Au NRs on the surface of TNWs/TNAs (Figure 4d). Typical EDS spectra collected from  $S_1$  and  $S_4$  shows Ti, O peaks for  $S_1$ , and Au, Ti, O peaks for  $S_4$ . Moreover, the elemental contents of  $S_1$  were  $[\text{Ti}] = 31.6 \pm 0.3 \text{ at.}\%$  and  $[\text{O}] = 68.4 \pm 0.3 \text{ at.}\%$ , while  $S_4$  had  $[\text{Au}] = 0.7 \pm 0.2 \text{ at.}\%$ ,  $[\text{Ti}] = 31.2 \pm 1.1 \text{ at.}\%$  and  $[\text{O}] = 68.1 \pm 1.3 \text{ at.}\%$ . The Ti and O contents had a relatively close stoichiometry of  $\text{TiO}_2$ . These EDS results suggest the successful fabrications of  $\text{TiO}_2$  and Au- $\text{TiO}_2$  films in this study (Figure 4f).



**Figure 4.** SEM images of (a) TNWs/TNAs ( $S_1$ ), (b) Au NPs-TNWs/TNAs ( $S_2$ ), (c) Au NRs-TNWs/TNAs ( $S_3$ ), and (d) Au NPs-NRs-TNWs/TNAs ( $S_4$ ). (e) A typical cross-sectional SEM image of the  $TiO_2$  films in this study. (f) The typical EDS spectra of  $S_1$  and  $S_4$  in this study.

The HRTEM image of  $S_4$  in Figure 5a shows Au NP and Au NR decorated onto  $TiO_2$ . To reveal the structural quality at the interface between Au/ $TiO_2$ , an HRTEM image obtained from the dashed square area in Figure 5a presents a sharp interface between Au NP-, Au NR- and  $TiO_2$  that facilitates the charge transfer to reduce the charge recombination (Figure 5b). In addition, the three crystallite domains have different orientations and lattice spacings of approximately 0.23 nm, 0.20 nm, and 0.35 nm, which correspond to the Au(111), Au (200) (AMCSD-0011140), and anatase  $TiO_2$  (101) planes (AMCSD-0019093), respectively. Thus, it is evidenced that the close contact metal-semiconductor (Au- $TiO_2$ ) heterostructure is successfully formed.



**Figure 5.** (a) An HRTEM image of Au-NPs-NRs-TNWs/TNAs ( $S_4$ ). (b) An HRTEM image obtained from the dashed square area in panel (a), showing the crystal structure at the interface of Au NP–Au NR and  $\text{TiO}_2$ .

To elucidate the chemical states, compositions, and functional groups on the surfaces of the studied nanomaterials, the XPS spectrum of a representative Au NPs-NRs-TNWs/TNAs film ( $S_4$ ) was measured. Figure 6a is a wide-scan XPS spectrum of  $S_4$ , which clearly shows the spectra of Au 4f, Ti 2p, and O 1s. In Figure 6b, Au 4f<sub>7/2</sub> peaks at 83.2 eV, which was lower than the Au 4f<sub>7/2</sub> at 84.0 eV of Au in the metallic state (see Figure 6a inset for confirming the Au binding energy) [2,39]. The Au 4f<sub>7/2</sub> peak exhibited a negative shift by 0.8 eV, which could be due to the electron transfer from oxygen vacancies of  $\text{TiO}_2$  to Au, suggesting the strong interaction between  $\text{TiO}_2$  and Au. This result agreed well with the results for the dendritic Au/ $\text{TiO}_2$  nanorod arrays [2] and Au/ $\text{TiO}_2$  nanotubes [40]. The C 1s presented a main peak at 184.8 eV of C=C and a small peak of O=C– at 188.3 eV, suggesting the formation of bond type O=C–O–Ti and C–O group (Figure 6c) [41]. In addition, according to the deconvolution results, Ti 2p<sub>1/2</sub> and Ti 2p<sub>3/2</sub> peaks were located at 464.4 eV and 458.7 eV, respectively (Figure 6d), indicating the Ti<sup>4+</sup> oxidation state [2,40,41]. As shown in Figure 6e, the O 1s spectrum is asymmetrical and it has an extending tail towards the higher energy. The O 1s was deconvoluted into three component peaks at 530.0 eV, 531.8 eV, and 533.7 eV, which could be assigned to (i) O<sup>2-</sup> in the  $\text{TiO}_2$  lattice, (ii) Ti–OH or C=O groups bound to two titanium atoms, (iii) OH groups bound to C and/or Ti, respectively [42,43].

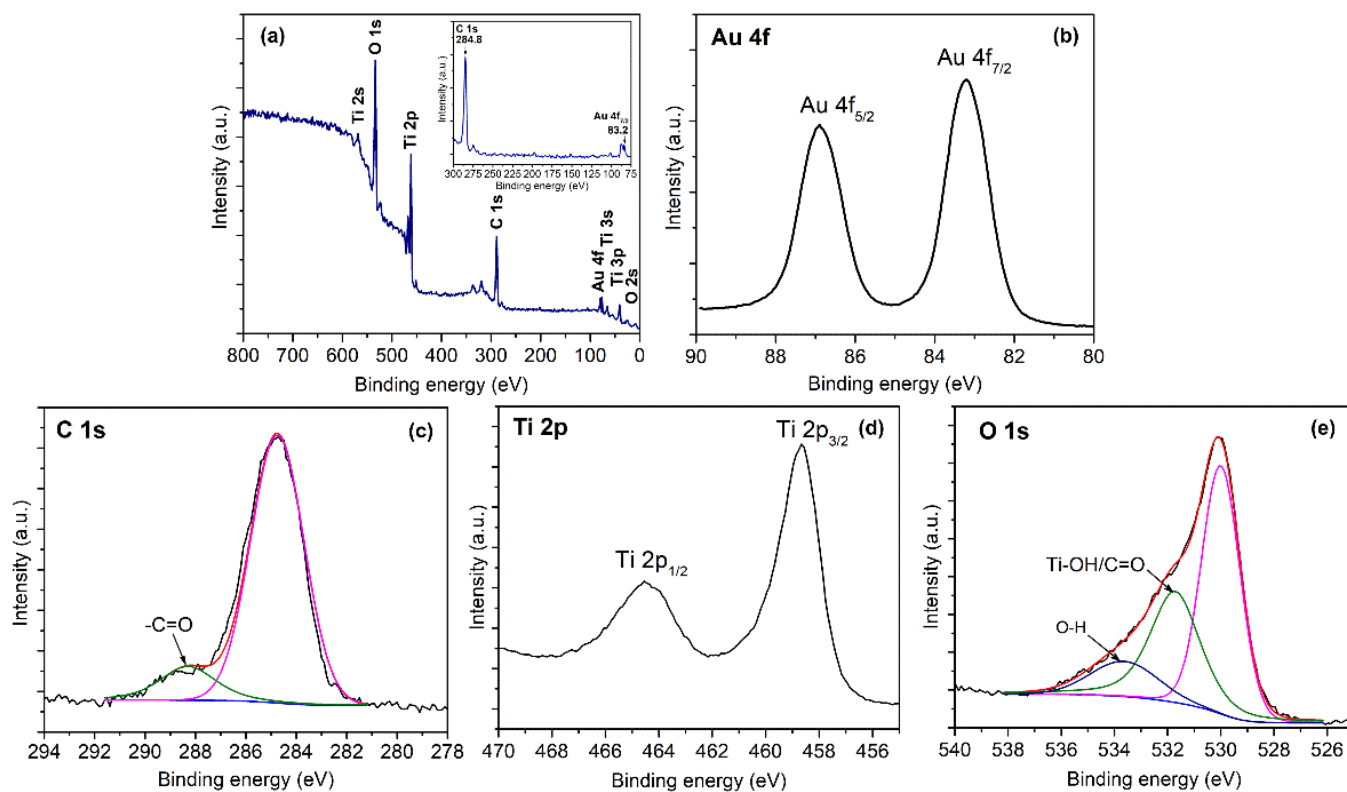


**Figure 6.** (a) Wide-scan XPS spectrum of Au NPs-NRs-TNWs/TNAs ( $S_4$ ); Inset shows Au 4f and C1s calibrated at 284.8 eV. High-resolution spectrum for (b) Au 4f; (c) C 1s; (d) Ti 2p; (e) O 1s.

To evaluate the PEC activity of TNWs/TNAs and Au-TNWs/TNAs, linear sweeping voltammetry (LSV) curves were performed using the sample as photoanode, Pt as a counter electrode, and Ag/AgCl as a reference electrode and under the UV-Vis irradiation. As shown in Figure 7a, without illumination, all the TNWs/TNAs and Au-TNWs/TNAs photoanodes exhibited negligible photocurrent density ( $J$ ) in the whole potential range [44]. The  $J$  increased remarkably for all the photoanodes with illumination, indicating typical properties of the semiconductor. Moreover, the  $J$  of Au-decorated TNWs/TNAs was remarkably higher than that of TNWs/TNAs photoanode. At 0.15 V, the  $J$  values of  $S_1$ ,  $S_2$ ,  $S_3$ , and  $S_4$  were 0.24, 0.32, 0.31, and 0.40 mA/cm<sup>2</sup>, respectively (Figure 7a). This means that Au NPs-NRs-TNWs/TNAs ( $S_4$ ) possessed the highest PEC activity among all the investigated photoanode nanomaterials.

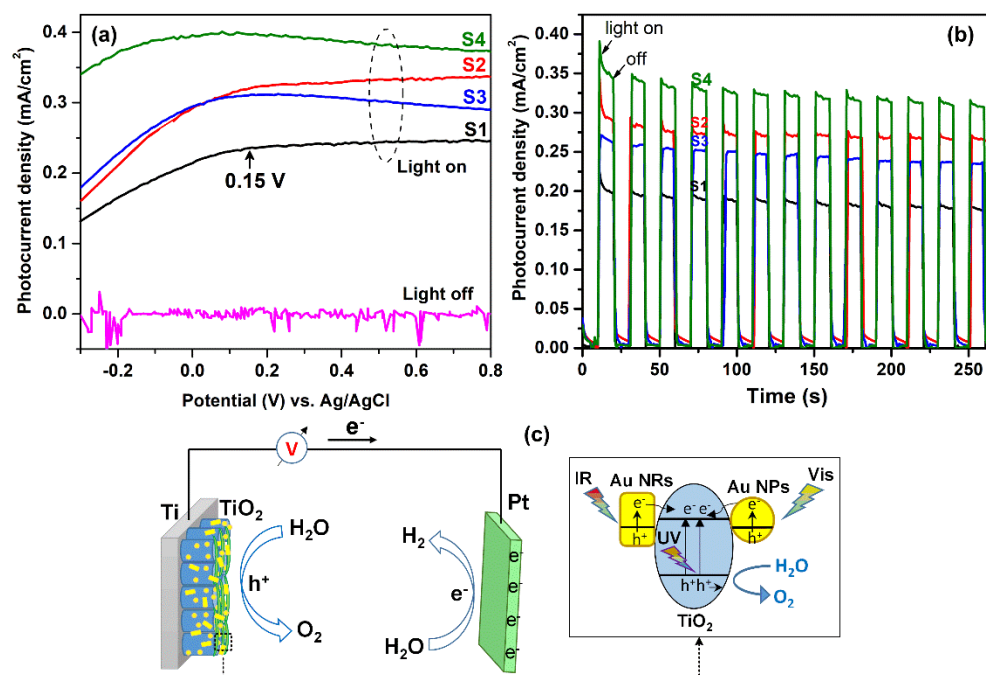


**Figure 7.** (a) Linear sweep voltammetry (LSV) of TNWs/TNAs and Au-TNWs/TNAs (S<sub>1</sub>–S<sub>4</sub>) recorded in a 0.5 M Na<sub>2</sub>SO<sub>4</sub> solution under the illumination of 100 W xenon lamp. (b) Chronoamperometric I–t curves for the samples collected at 0.15 V versus RHE under the UV-Vis irradiation of 100 W xenon lamp. (c) A schematic illustration for PEC water splitting using Au NPs-NRs-TNWs/TNAs array as a photoanode.

Table 1 summarizes the photocurrent densities of the optimal Au-TiO<sub>2</sub>-based photoanodes developed in this study and in the literature [45–49]. The *J* of the Au NPs-NRs-TiO<sub>2</sub> photoanode (0.4 mA/cm<sup>2</sup>) was higher than that of Au/reduced graphene oxide/hydrogenated TiO<sub>2</sub> nanotube arrays (Au/RGO/H-TNTs, 0.22 mA/cm<sup>2</sup>) under the visible light irradiation [45], but it was 2.4–6.8 times lower than the optimum *J* values of Au/TiO<sub>2</sub>/Au heterostructure (0.94 mA/cm<sup>2</sup>) [46], Au/TiO<sub>2</sub> nanorod arrays (1.1 mA/cm<sup>2</sup>) [47], Au NPs-NRs/TiO<sub>2</sub> nanowires (1.49 mA/cm<sup>2</sup>) [11], Au NPs- branched TiO<sub>2</sub> (2.5 mA/cm<sup>2</sup>) [48], and Au NPs/ 3D TiO<sub>2</sub> nanorods (2.7 mA/cm<sup>2</sup>) [49]. The different *J* values from different studies are attributed to both the intrinsic different PEC properties of the photoanodes and the different PEC experimental conditions (e.g., light source, potential, and electrolyte).

**Table 1.** Photocurrent density and photoelectrochemical measurement conditions of the optimal Au/TiO<sub>2</sub>-based photoanodes developed in this study and in the literature.

Photoanode Nanomaterial	Electrolyte/Potential (V) vs. RHE	Illumination	Photocurrent Density (mA/cm <sup>2</sup> )	Ref.
Au NPs-NRs/TNWs/TNAs	0.5 M Na <sub>2</sub> SO <sub>4</sub> /0.15 V	100 W Xe lamp	0.40	This study
Au/RGO/H-TNTs	1 M KOH/1.23 V	Xe lamp, AM 1.5G filter, λ > 400 nm	0.22	[45]
Au/TiO <sub>2</sub> /Au heterostructure	1 M KOH/0.2 V	300 W Xenon Lamp, 100 mW/cm <sup>2</sup> UV–100 mW/cm <sup>2</sup> Vis	0.94	[46]
Au/TiO <sub>2</sub> nanorod arrays	0.5 M Na <sub>2</sub> SO <sub>4</sub> /1.0 V	500 W Xe lamp, 100 mW/cm <sup>2</sup>	1.1	[47]
Au NPs-NRs/TiO <sub>2</sub> nanowires	1 M KOH/0 V	AM 1.5G, 100 mW/cm <sup>2</sup>	1.49	[11]
Au NPs-branched TiO <sub>2</sub>	0.5 M Na <sub>2</sub> SO <sub>4</sub> /1.23 V	500 W Xe lamp, 100 mW/cm <sup>2</sup>	2.5	[48]
Au NPs/3D TiO <sub>2</sub> nanorods	1 M NaOH/0 V	150 W Xe lamp, AM 1.5G, 100 mW/cm <sup>2</sup>	2.7	[49]

Figure 7c presents a schematic diagram of a possible PEC water-splitting process for Au NPs-NRs-TNWs/TNAs. The photoanode exhibited an enhanced PEC activity owing to the following factors: (1) the LSPR of Au NPs and Au NRs improve the light-harvesting capability and the light absorption in both Vis and IR regions (Figures 3c,d and 9a), (2) the enhancement of photogenerated carriers' density due to LSPR at Au NPs and Au NRs, (3) the LSPR hot electrons ( $e^-$ ) in Au NPs and Au NRs can inject into the conduction band of  $\text{TiO}_2$  to improve the electrons' injection efficiency and reduce electron-hole recombination rate [48]. Therefore, these synergistic effects of Au NPs-NRs-TNWs/TNAs resulted in the highest PEC performance over either the single-type Au-decorated TNWs/TNAs or the pristine TNWs/TNAs.

The photocurrent response graphs at 0.15 V of the photoanodes with controlling of the on-off irradiation cycle are shown in Figure 7b. The measured  $J$  values were exactly consistent with those recorded in the LSV experiments at 0.15 V. Based on the  $J$  values, the PEC performance of the four photoanode nanomaterials was in the order of  $S_4 > S_2 > S_3 > S_1$ . Furthermore, though witnessing a considerable photocurrent drop in the first 25 s, the photocurrent remained relatively stable during the test lasting 270 s, with only a 13%  $J$  decrease with respect to the maximum  $J$  value.

Since  $S_4$  possessed the highest PEC activity, it was of interest to further study its photocatalytic activity in the degradation of MB. Figure 8a,b show MB degradation by photolysis and photocatalysis using  $S_1$  and  $S_4$  under the UV-Vis irradiation of a 100 W xenon lamp. It is seen that the main MB absorbance at  $\lambda_{\text{max}} \sim 659$  nm decreases substantially with the increase in the irradiation time (Figure 8c). Clearly, both photolysis and photocatalysis induced the decrease of MB concentration with the exponential decay,  $C_t = C_0 \times e^{-kt}$ , where  $C_0$  is the initial concentration,  $C_t$  is the concentration of MB at time  $t$ , and  $k$  is the reaction rate constant ( $\text{h}^{-1}$ ). In Figure 8d, the  $k$  is obtained by performing the linear fitting on the plot of  $-\ln(C_t/C_0)$  vs.  $t$ . Specifically, the  $k$  of the photolysis process was a low value of  $0.13 \text{ h}^{-1}$ , indicating that MB is quite stable under UV-Vis irradiation (Figure 8d inset). Meanwhile, under the photocatalytic reactions, the  $k$  values of  $S_1$  and  $S_4$  were  $0.28 \pm 0.02 \text{ h}^{-1}$  and  $0.70 \pm 0.07 \text{ h}^{-1}$ , respectively (Figure 8d inset). This means that the  $k$  value of Au NPs-NRs-TNWs/TNAs was 2.5 times higher than that of TNWs/TNAs, which indicates a dramatic enhancement in the photocatalytic activity of  $\text{TiO}_2$  by introducing a mixture of Au NPs and Au NRs.

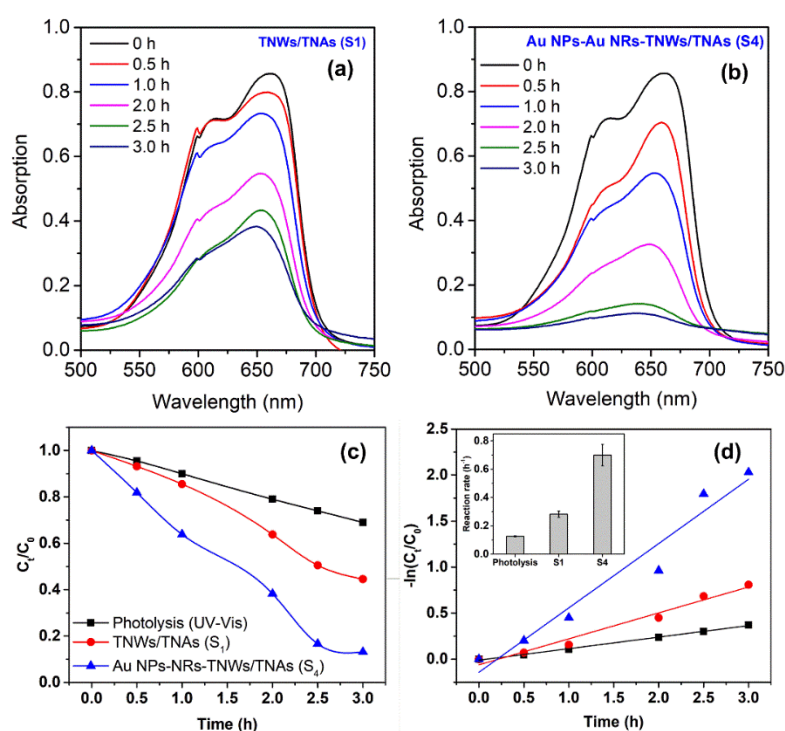


**Figure 8.** (a,b) Changes in UV-visible absorption spectra of MB by TNWs/TNAs ( $S_1$ ) and Au NPs-NRs- TNWs/TNAs ( $S_4$ ) as a function of irradiation time. (c,d) Variations in ( $C_t/C_0$ ) and  $-\ln(C_t/C_0)$  as a function of irradiation time. Inset in (d) is the reaction rate constant ( $k$ ) of  $S_1$  and  $S_4$ .

For reference, Table 2 summarizes the  $k$  values of TiO<sub>2</sub>-based nanophotocatalysts prepared by some methods in this study and the relevant literature [10,50–53]. It is very hard to make the right comparison when each developed TiO<sub>2</sub>-based nanophotocatalyst has its intrinsic properties (e.g., morphology-surface area, crystal structure, composition, decoration, or doping content) and different photocatalytic reaction conditions (e.g., catalyst dosage, light source, initial concentration of MB). Generally, the  $k$  value of the present TNWs/TNAs ( $0.28\text{ h}^{-1}$ ) was twice higher than those of the 40 nm-TNAs/ 20 nm-TNWs ( $0.13\text{ h}^{-1}$ ) and the TiO<sub>2</sub> nanoparticles film ( $0.14\text{ h}^{-1}$ ) in ref. [10], which could be due to the larger surface area associated with the thicker TNAs and longer TNWs film in this study. Meanwhile, the  $k$  value of Au NPs-NRs- TNWs/TNAs ( $0.7\text{ h}^{-1}$ ) was comparable with those of the optimal Ag/TiO<sub>2</sub> nanoparticles ( $0.65\text{ h}^{-1}$ ) [50] and the Bi-Fe doped TiO<sub>2</sub> ( $0.78\text{ h}^{-1}$ ) [51]. However, the  $k$  value of Au NPs-NRs- TNWs/TNAs was 2.1–2.7 times lower than the  $k$  values of the brookite phase TNAs ( $1.45\text{ h}^{-1}$ ) synthesized by anodization and annealed at 500 °C [53], and of the SnO<sub>2</sub> NPs-decorated TNAs ( $1.86\text{ h}^{-1}$ ) prepared by anodization and solvothermal process [52].

**Table 2.** The synthesis methods and photocatalytic reaction rate constants in the degradation of methylene of the selected TiO<sub>2</sub>-based nanophotocatalysts in this study and the literature.

Photocatalyst	Synthesis Methods	Reaction Rate ( $\text{h}^{-1}$ )	Ref.
TNWs/TNAs	Anodization	$0.28 \pm 0.02$	This study
Au NPs-NRs/TNWs/TNAs	Turkevick method–anodization–drop casting method	$0.70 \pm 0.07$	This study
40 nm-TNWs/20 nm-TNAs	Anodic oxidation	0.13	[10]
TiO <sub>2</sub> nanoparticles P25 film	-	0.14	[10]
TNAs	Anodization	1.45	[53]
Ag/TiO <sub>2</sub> P25	Photo-reduction method	0.65	[50]
Bi-Fe doped TiO <sub>2</sub>	Wet impregnation technique	0.78	[51]
SnO <sub>2</sub> NPs-decorated TNAs	Anodization–solvothermal process	1.86	[52]

To elucidate the mechanism of the photocatalytic activity enhancement in Au NPs-NRs-TNWs/TNAs, the absorption spectra of  $S_1$  and  $S_4$  were measured and shown in Figure 9a. Obviously, the TNWs/TNAs exhibited a typical absorption spectrum of TiO<sub>2</sub>, characterized by a gradually increased absorbance in the IR-Vis region and a sharply increased absorbance in the UV region. Meanwhile, Au NPs-NRs-TNWs/TNAs had an LSPR peak of Au NPs at approximately 512 nm, and a broad intense absorption peak at 1192 nm owing to the LSPR peak of Au NRs.

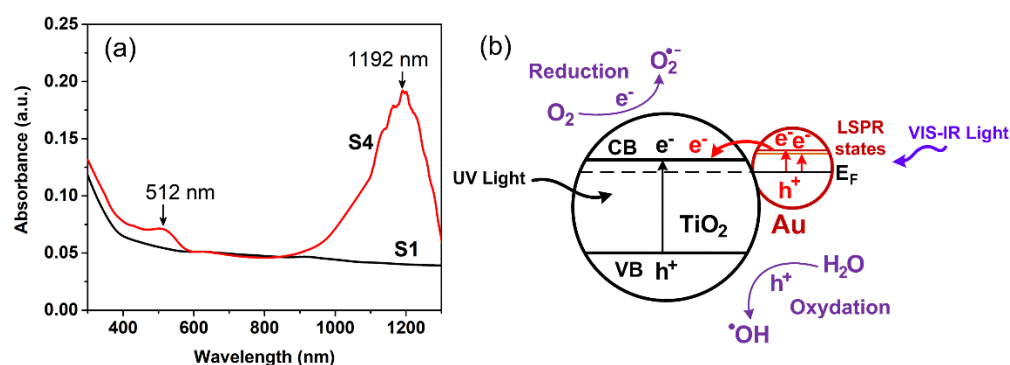


**Figure 9.** (a) Absorption spectra of the solution of S<sub>1</sub> and S<sub>4</sub> prepared by scratching 1 mg powder of TNWs/TNAs and Au-TNWs/TNAs. (b) A proposed mechanism for the photocatalytic activity of Au-TiO<sub>2</sub> upon the excitation of the Au surface plasmon band.

As shown in Figure 9b, a proposed mechanism of the significant *k* enhancement by decorating TNWs/TNAs with Au NPs and Au NRs is due to the LSPR effect [11,25,28,54,55]. In fact, the LSPR peaks at 112 nm for Au NPs and 1192 nm for Au NRs were observed, as shown in Figures 3c,d, and 7a. For describing LSPR, when the electromagnetic field of the incident light becomes associated with the oscillations of the conduction electrons of Au NPs and Au NRs, the local electromagnetic fields near the surface of Au NPs and Au NRs enhanced strongly [11,23]. Indeed, by 3D finite-difference time-domain simulation, the electrical field amplification at the Au/TiO<sub>2</sub> interfaces upon SPR excitation was observed clearly [11,23,49]. Therefore, the enhanced photocatalytic activity of Au NPs-NRs-TiO<sub>2</sub> in this study is attributed to the LSPR absorption of Au NPs and Au NRs under Vis-IR illumination to generate photoexcited electrons in LSPR states and holes. Then, the energetic electrons can inject into the conduction band of TiO<sub>2</sub> that leads to the enhanced separation of photo-excited electron-hole pairs, and generate a larger amount of reactive oxygenated free radicals (e.g., O<sub>2</sub><sup>•-</sup> and •OH) to trigger photocatalytic reactions (Figure 9b) [15,28,38,56,57]. Since Au NPs-NRs-TNWs/TNAs obtained the LSPR-absorption in both Vis and IR regions, they achieved the best PEC activity among the four nanomaterials and presented a high photocatalytic performance. It is worth mentioning that a further study on Au NPs-NRs-TNWs/TNAs with different Au NPs- and Au NRs-sizes, amounts, and mixing ratios is of great interest to further enhance the PEC and photocatalytic properties of the nanomaterial.

#### 4. Conclusions

TNWs/TNAs and Au-TNWs/TNAs nanomaterials were successfully synthesized by the anodic oxidation method combined with a chemical reduction method, and their PEC and photocatalytic activities were studied. The TNWs/TNAs and Au-TNWs/TNAs exhibited pure anatase phase of TiO<sub>2</sub> with (0 0 4), (1 0 1), and (1 0 5) preferred orientations, and componential Au (111) peak was observed for Au-TNWs/TNAs. The samples presented well-defined and uniform structure of TNWs/TNAs (i.e., TiO<sub>2</sub> nanowire length of ~6.0 μm covering on TiO<sub>2</sub> nanotubes arrays with tube diameter of ~80 nm and tube length of ~6.0 μm). Additionally, sharp Au/TiO<sub>2</sub> interfaces were observed via HRTEM images, and XPS results confirm for the strong interaction Au-TiO<sub>2</sub>, the Ti<sup>4+</sup> oxidation state, and the typical functional groups on the material surfaces. In addition, Au NPs (size of 19.0 ± 1.9 nm) and Au NRs (width of 14.8 ± 1.3 nm and length of 99.8 ± 15.1 nm) were relatively even decoration on TNWs/TNAs. The EDS results show that Au-decorated content onto TiO<sub>2</sub> was 0.7 ± 0.2 at.%. For PEC properties, the photocurrent density (J) at 0.15 V was 0.24 mA/cm<sup>2</sup> for TNWs/TNAs, 0.32 mA/cm<sup>2</sup> for Au NRs-TNWs/TNAs, 0.31 mA/cm<sup>2</sup> for Au NPs-TNWs/TNAs, and 0.40 mA/cm<sup>2</sup> for Au NRs-NRs-TNWs/TNAs. This means that Au NRs-NRs-TNWs/TNAs achieved the best PEC activity owing to the LSPR-absorption of Au NPs and Au NRs in the Vis and IR regions. Furthermore, Au NPs-NRs-TNWs/TNAs possessed a high photocatalytic performance in MB degradation with *k* = 0.7 h<sup>-1</sup>, which was 2.5 times higher than that of the pristine TNWs/TNAs. These study results demonstrate that the PEC and photocatalytic properties of semiconductors can be enhanced by combining various nanostructures of plasmonic noble metals.

**Author Contributions:** N.N.U. performed the experiments, analyzed the data, and wrote the first paper-draft; P.H.L., L.A.T. revised and edited the paper and supervised the study; P.H.L. was project administrator and funding acquisition. L.T.C.T., L.T.H. and H.P.T. contributed to the material characterizations. T.T.T.N., T.C.M.V.D., K.T.N., N.T.N.H. and S.-R.J. contributed to the useful discussions and reviewed the paper. S.-R.J., and C.-W.L. supported for the advanced characterizations and review and made minor revisions to the paper. All authors have read and agreed to the published version of the manuscript.

**Funding:** This research is funded by Vietnam National Foundation for Science and Technology Development (NAFOSTED) under grant number 103.02-2019.374.

**Institutional Review Board Statement:** Not applicable.

**Informed Consent Statement:** Not applicable.

**Data Availability Statement:** Not applicable.

**Acknowledgments:** The authors acknowledge the support of time and facilities from Ho Chi Minh City University of Technology-VNU-HCM, National Yang Ming Chiao Tung University, and Can Tho University of Medicine and Pharmacy for this study.

**Conflicts of Interest:** The authors declare no conflict of interest.

## References

1. Fujishima, A.; Honda, K. Electrochemical photolysis of water at a semiconductor electrode. *Nature* **1972**, *238*, 37–38.
2. Su, F.; Wang, T.; Lv, R.; Zhang, J.; Zhang, P.; Lu, J.; Gong, J. Dendritic Au/TiO<sub>2</sub> nanorod arrays for visible-light driven photoelectrochemical water splitting. *Nanoscale* **2013**, *5*, 9001.
3. Houas, A.; Lachheb, H.; Ksibi, M.; Elaloui, E.; Guillard, C.; Herrmann, J.-M. Photocatalytic degradation pathway of methylene blue in water. *Appl. Catal. B* **2001**, *31*, 145–157.
4. Hoffmann, M.R.; Martin, S.T.; Choi, W.Y.; Bahnemann, D.W. Environmental Applications of Semiconductor Photocatalysis. *Chem. Rev.* **1995**, *95*, 69–96.
5. Asahi, R.; Morikawa, T.; Irie, H.; Ohwaki, T. Nitrogen-doped titanium dioxide as visible-light-sensitive photocatalyst: Designs, developments, and prospects. *Chem. Rev.* **2014**, *114*, 9824–9852.
6. Chen, X.; Mao, S.S. Titanium Dioxide Nanomaterials: Synthesis, Properties, Modifications, and Applications. *Chem. Rev.* **2007**, *107*, 2891–2959.
7. Singh, J.; Manna, A.K.; Soni, R.K. Bifunctional Au–TiO<sub>2</sub> thin films with enhanced photocatalytic activity and SERS based multiplexed detection of organic pollutant. *J. Mater. Sci. Mater. Electron.* **2019**, *30*, 16478–16493.
8. Hoang, S.; Guo, S.; Hahn, N.T.; Bard, A.J.; Mullins, C.B. Visible Light Driven Photoelectrochemical Water Oxidation on Nitrogen-Modified TiO<sub>2</sub> Nanowires. *Nano Lett.* **2012**, *12*, 26–32.
9. Baker, D.R.; Kamat, P.V. Photosensitization of TiO<sub>2</sub> Nanostructures with CdS Quantum Dots: Particulate versus Tubular Support Architectures. *Adv. Funct. Mater.* **2009**, *46556*, 805–811.
10. Hsu, M.-Y.; Hsu, H.-L.; Leu, J. TiO<sub>2</sub> Nanowires on Anodic TiO<sub>2</sub> Nanotube Arrays (TNWs/TNAs): Formation Mechanism and Photocatalytic Performance. *J. Electrochem. Soc.* **2012**, *159*, H722–H727.
11. Pu, Y.C.; Wang, G.; Chang, K.-D.; Ling, Y.; Lin, Y.K.; Fitzmorris, B.C.; Liu, C.M.; Lu, X.; Tong, Y.; Zhang, J.Z.; et al. Au nanostructure-decorated TiO<sub>2</sub> nanowires exhibiting photoactivity across entire UV-visible region for photoelectrochemical water splitting. *Nano Lett.* **2013**, *13*, 3817–3823.
12. Mo, S.-D.; Ching, W.Y. Electronic and optical properties of three phases of titanium dioxide: Rutile, anatase, and brookite. *Phys. Rev. B.* **1995**, *51*, 13023.
13. Khan, M.A.M.; Siwach, R.; Kumar, S.; Alhazaa, A.N. Role of Fe doping in tuning photocatalytic and photoelectrochemical properties of TiO<sub>2</sub> for photodegradation of methylene blue. *Opt. Laser Technol.* **2019**, *118*, 170–178.
14. Do, T.C.M.V.; Nguyen, D.Q.; Nguyen, K.T.; Le, P.H. TiO<sub>2</sub> and Au-TiO<sub>2</sub> Nanomaterials for Rapid Photocatalytic Degradation of Antibiotic Residues in Aquaculture Wastewater. *Materials* **2019**, *12*, 2434.
15. Lincic, S.; Christopher, P.; Ingram, D.B. Plasmonic-metal nanostructures for efficient conversion of solar to chemical energy. *Nat. Mater.* **2011**, *10*, 911–921.
16. Yu, Y.; Wen, W.; Qian, X.-Y.; Liu, J.-B.; Wu, J.-M. UV and visible light photocatalytic activity of Au/TiO<sub>2</sub> nanoforests with Anatase/Rutile phase junctions and controlled Au locations. *Sci. Rep.* **2017**, *7*, 41253.
17. Zhang, J.; Jin, X.; Morales-guzman, P.I.; Yu, X.; Liu, H.; Zhang, H.; Razzari, L.; Claverie, J.P. Engineering the Absorption and Field Enhancement Properties of Au–TiO<sub>2</sub> Nanohybrids via Whispering Gallery Mode Resonances for Photocatalytic Water Splitting. *ACS Nano* **2016**, *10*, 4496–4503.
18. Luo, J.; Ma, L.; He, T.; Ng, C.F.; Wang, S.; Sun, H.; Fan, H.J. TiO<sub>2</sub>/(CdS, CdSe, CdSeS) Nanorod Heterostructures and Photoelectrochemical Properties. *J. Phys. Chem. C* **2012**, *116*, 11956–11963.
19. Lin, H.; Mao, Z.; Zhou, N.; Wang, M.; Li, L.; Li, Q. Fabrication of CdS quantum dots sensitized TiO<sub>2</sub> nanowires/nanotubes arrays and their photoelectrochemical properties. *SN Appl. Sci.* **2019**, *1*, 391.
20. Kelly, K.L.; Coronado, E.; Zhao, L.L.; Schatz, G.C. The Optical Properties of Metal Nanoparticles: The Influence of Size, Shape, and Dielectric Environment. *J. Phys. Chem. B.* **2003**, *107*, 668–677.
21. Chou, C.-H.; Chen, C.-D.; Wang, C.R.C. Highly Efficient, Wavelength-Tunable, Gold Nanoparticle Based Optothermal Nanoconvertors. *J. Phys. Chem. B.* **2005**, *109*, 11135–11138.

22. Li, C.; Shuford, K.L.; Chen, M.; Lee, E.J.; Cho, S.O. A Facile Polyol Route to Uniform Gold Octahedra with Tailorable Size and Their Optical Properties. *ACS Nano* **2008**, *2*, 1760.
23. Liu, Z.; Hou, W.; Pavaskar, P.; Aykol, M.; Cronin, S.B. Plasmon Resonant Enhancement of Photocatalytic Water Splitting Under Visible Illumination. *Nano Lett.* **2011**, *11*, 1111–1116.
24. Paul, K.K.; Giri, P.K. Role of Surface Plasmons and Hot Electrons on the Multi-Step Photocatalytic Decay by Defect Enriched Ag@TiO<sub>2</sub> Nanorods Under Visible Light Illumination. *J. Phys. Chem. C* **2017**, *121*, 20016–20030.
25. Wang, C.; Astruc, D. Nanogold plasmonic photocatalysis for organic synthesis and clean energy conversion. *Chem. Soc. Rev* **2014**, *43*, 7188.
26. Singh, J.; Sahu, K.; Satpati, B.; Shah, J.; Kotnala, R.K.; Mohapatra, S. Facile synthesis, structural and optical properties of Au-TiO<sub>2</sub> plasmonic nanohybrids for photocatalytic applications. *J. Phys. Chem. Solids* **2019**, *135*, 109100.
27. Fu, F.; Zhang, Y.; Zhang, Z.; Zhang, X.; Chen, Y.; Zhang, Y. The preparation and performance of Au loads TiO<sub>2</sub> nanomaterials. *Mater. Res. Express* **2019**, *6*, 095041.
28. Veziroglu, S.; Ullrich, M.; Hussain, M.; Drewes, J.; Shondo, J.; Strunskus, T.; Adam, J.; Faupel, F.; Aktas, O.C. Plasmonic and non-plasmonic contributions on photocatalytic activity of Au-TiO<sub>2</sub> thin film under mixed UV–Visible light. *Surf. Coat. Technol.* **2020**, *389*, 125613.
29. Link, S.; Mohamed, M.B.; El-Sayed, M.A. Simulation of the Optical Absorption Spectra of Gold Nanorods as a Function of Their Aspect Ratio and the Effect of the Medium Dielectric Constant. *J. Phys. Chem. B* **1999**, *103*, 3073–3077.
30. Sau, T.K.; Murphy, C.J. Seeded High Yield Synthesis of Short Au Nanorods in Aqueous Solution. *Langmuir* **2004**, *20*, 6414–6420.
31. Kumar, R.; Binetti, L.; Nguyen, T.H.; Alwis, L.S.M.; Agrawal, A.; Sun, T.; Grattan, K.T.V. Determination of the Aspect-ratio Distribution of Gold Nanorods in a Colloidal Solution using UV-visible absorption spectroscopy. *Sci. Rep.* **2019**, *9*, 17469.
32. Enustun, B.V.; Turkevich, J. Coagulation of Colloidal Gold. *J. Am. Chem. Soc.* **1963**, *85*, 3317–3328.
33. Kimling, J.; Maier, M.; Okenve, B.; Kotaidis, V.; Ballot, H.; Plech, A. Turkevich Method for Gold Nanoparticle Synthesis Revisited. *J. Phys. Chem. B* **2006**, *110*, 15700–15707.
34. Sun, L.; Cai, J.; Wu, Q.; Huang, P.; Su, Y.; Lin, C. N-doped TiO<sub>2</sub> nanotube array photoelectrode for visible-light-induced photoelectrochemical and photoelectrocatalytic activities. *Electrochim. Acta* **2013**, *108*, 525–531.
35. Preethi, L.K.; Antony, R.P.; Mathews, T.; Walczak, L.; Gopinath, C.S. A Study on Doped Heterojunctions in TiO<sub>2</sub> Nanotubes: An Efficient Photocatalyst for Solar Water Splitting. *Sci. Rep.* **2017**, *7*, 14314.
36. Do, T.C.M.V.; Nguyen, D.Q.; Nguyen, T.D.; Le, P.H. Development and Validation of a LC-MS/MS Method for Determination of Multi-Class Antibiotic Residues in Aquaculture and River Waters, and Photocatalytic Degradation of Antibiotics by TiO<sub>2</sub> Nanomaterials. *Catalysts* **2020**, *10*, 356.
37. Tuyen, L.T.C.; Jian, S.-R.; Tien, N.T.; Le, P.H. Nanomechanical and Material Properties of Fluorine-Doped Tin Oxide Thin Films Prepared by Ultrasonic Spray Pyrolysis: Effects of F-Doping. *Materials* **2019**, *12*, 1665.
38. Chen, Y.; Bian, J.; Qi, L.; Liu, E.; Fan, J. Efficient Degradation of Methylene Blue over Two-Dimensional Au/TiO<sub>2</sub> Nanosheet Films with Overlapped Light Harvesting Nanostructures. *J. Nanomater.* **2015**, *2015*, 905259.
39. Padikkaparambil, S.; Narayanan, B.; Yaakob, Z.; Viswanathan, S.; Tasirin, S.M. Au/TiO<sub>2</sub> Reusable Photocatalysts for Dye Degradation. *Inter. J. Photoenergy* **2013**, *2013*, 752605.
40. Liu, W.; Duan, W.; Jia, L.; Wang, S.; Guo, Y.; Zhang, G.; Zhu, B.; Huang, W.; Zhang, S. Surface Plasmon-Enhanced Photoelectrochemical Sensor Based on Au Modified TiO<sub>2</sub> Nanotubes. *Nanomaterials* **2022**, *12*, 2058.
41. Kruse, N.; Chenakin, S. XPS characterization of Au/TiO<sub>2</sub> catalysts: Binding energy assessment and irradiation effects. *Appl. Catal. A* **2011**, *391*, 367–376.
42. Yoshiiri, K.; Wang, K.; Kowalska, E. TiO<sub>2</sub>/Au/TiO<sub>2</sub> Plasmonic Photocatalysts: The Influence of Titania Matrix and Gold Properties. *Inventions* **2022**, *7*, 54.
43. Yu, J.; Zhao, X.; Zhao, Q. Effect of surface structure on photocatalytic activity of TiO<sub>2</sub> thin films prepared by sol-gel method. *Thin Solid Films* **2000**, *379*, 7–14.
44. Xu, F.; Mei, J.; Li, X.; Sun, Y.; Wu, D.; Gao, Z.; Zhang, Q.; Jiang, K. Heterogeneous three-dimensional TiO<sub>2</sub>/ZnO nanorod array for enhanced photoelectrochemical water splitting properties. *J. Nanopart Res.* **2017**, *19*, 297.
45. Luo, J.; Li, D.; Yang, Y.; Liu, H.; Chen, J.; Wang, H. Preparation of Au/reduced graphene oxide/hydrogenated TiO<sub>2</sub> nanotube arrays ternary composites for visible-light-driven photoelectrochemical water splitting. *J. Alloys Compd.* **2016**, *661*, 380–388.
46. Li, Y.; Yu, H.; Zhang, C.; Fu, L.; Li, G.; Shao, Z.; Yi, B. Enhancement of photoelectrochemical response by Au modified in TiO<sub>2</sub> nanorods. *Int. J. Hydrogen Energy* **2013**, *38*, 13023–13030.
47. Xu, F.; Bai, D.; Mei, J.; Wu, D.; Gao, Z.; Jiang, K.; Liu, B. Enhanced photoelectrochemical performance with in-situ Au modified TiO<sub>2</sub> nanorod arrays as photoanode. *J. Alloys Compd.* **2016**, *688*, 914–920.
48. Xu, F.; Mei, J.; Zheng, M.; Bai, D.; Wu, D.; Gao, Z.; Jiang, K. Au nanoparticles modified branched TiO<sub>2</sub> nanorod array arranged with ultrathin nanorods for enhanced photoelectrochemical water splitting. *J. Alloys Compd.* **2017**, *693*, 1124–1132.
49. Li, H.; Li, Z.; Yu, Y.; Ma, Y.; Yang, W.; Wang, F.; Yin, X.; Wang, X. Surface-Plasmon-Resonance-Enhanced Photoelectrochemical Water Splitting from Au-Nanoparticle-Decorated 3D TiO<sub>2</sub> Nanorod Architectures. *J. Phys. Chem. C* **2017**, *121*, 12071–12079.

50. Tseng, H.-C.; Chen, Y.-W. Facile Synthesis of Ag/TiO<sub>2</sub> by Photoreduction Method and Its Degradation Activity of Methylene Blue under UV and Visible Light Irradiation. *Mod. Res. Catal.* **2020**, *9*, 1–19.
51. Mishra, S.; Chakinala, N.; Chakinala, A.G.; Surolia, P.K. Photocatalytic degradation of methylene blue using monometallic and bimetallic Bi-Fe doped TiO<sub>2</sub>. *Catal. Commun.* **2022**, *171*, 106518.
52. Li, Y.; Zhang, X.; Hu, X.; Li, Z.; Fan, J.; Liu, E. Facile fabrication of SnO<sub>2</sub>/TiO<sub>2</sub> nanotube arrays for efficient degradation of pollutants. *Opt. Mater.* **2022**, *127*, 112252.
53. Kang, X.; Chen, S. Photocatalytic reduction of methylene blue by TiO<sub>2</sub> nanotube arrays: Effects of TiO<sub>2</sub> crystalline phase. *J. Mater. Sci.* **2010**, *45*, 2696–2702.
54. Chen, Y.; Tian, G.; Pan, K.; Tian, C.; Zhou, J.; Zhou, W.; Ren, Z.; Fu, H. In situ controlled growth of well-dispersed gold nanoparticles in TiO<sub>2</sub> nanotube arrays as recyclable substrates for surface-enhanced Raman scattering. *Dalt. Trans.* **2012**, *41*, 1020–1026.
55. Zhang, Z.; Zhang, L.; Hedhili, M.N.; Zhang, H.; Wang, P. Plasmonic gold nanocrystals coupled with photonic crystal seamlessly on TiO<sub>2</sub> nanotube photoelectrodes for efficient visible light photoelectrochemical water splitting. *Nano Lett.* **2013**, *13*, 14–20.
56. Kowalska, E.; Mahaney, O.O.P.; Abe, R.; Ohtani, B. Visible-light-induced photocatalysis through surface plasmon excitation of gold on titania surfaces. *Phys. Chem. Chem. Phys.* **2010**, *12*, 2344–2355.
57. Nosaka, Y.; Nosaka, A. Understanding Hydroxyl Radical (\*OH) Generation Processes in Photocatalysis. *ACS Energy Lett.* **2010**, *1*, 356–359.